

Supporting Information

Production of propyl 4-hydroxybenzoate *via* selective hydrogenolysis of lignin catalyzed by Ni/MFI-ns

Lixia Li ^{a,b}, Yinan Rao ^a, Menghao Jiang ^a and Jinxing Long ^{a*}

^a School of Chemistry and Chemical Engineering, State Key Laboratory of Pulp and Paper Engineering, South China University of Technology, 510640, China

^b Collaborative Innovation Center of Henan Province for Green Manufacturing of Fine Chemicals, Key Laboratory of Green Chemical Media and Reactions, Ministry of Education, School of Chemistry and Chemical Engineering, Henan Normal University, Xinxiang, 453007, Henan, China.

Reagents and Materials

Nickel nitrate hexahydrate ($\text{Ni}(\text{NO}_3)_2 \cdot 6\text{H}_2\text{O}$, 99.5%), sulfuric acid (H_2SO_4 , 98%),

ethanol (99.7%), ethyl ether (AR), acetonitrile (99.9%), tetrahydrofuran (THF, 99.5%), and methylbenzene (AR) were obtained from Guangdong Guanghua Sci-Tech Co., Ltd. Aluminum sulfate ($\text{Al}_2(\text{SO}_4)_3 \cdot 18\text{H}_2\text{O}$, 99.0%), tetraethoxysilane (TEOS, AR), 1-bromodococane (99.0% AR), 1-bromohexane (AR), and N,N,N',N'-tetramethyl-1,6-diaminohexane, 2-phenoxy-1-phenylethanol (98.0%), 2-phenylethyl phenylacetate (>97.0%), dibenzyl ether (95.0%), benzyl phenyl ether (>98.0%), diphenylmethane (99.0%), ethyl 4-hydroxyhydrocinnamate (99.0%) and *p*-hydroxybenzoic acid (98.0%) were purchased from Aladdin Co., Ltd. All reagents are of analytical grade and were used without further purification. Bagasse, pine, cornstalk, poplar, poplar and corncob were obtained from Guangdong province, China.

Catalyst Preparations

The lamellar MFI-nanosheet (MFI-ns) was synthesized using an organic surfactant functionalized with a diquatery ammonium compound, $[\text{C}_{22}\text{H}_{45}\text{-N}^+(\text{CH}_3)_2\text{-C}_6\text{H}_{12}\text{-N}^+(\text{CH}_3)_2\text{-C}_6\text{H}_{13}]\text{Br}_2$ ($\text{C}_{22-6-6}\text{Br}_2$), as the structure-directing agent (SDA), following a procedure described in detail elsewhere¹⁻³. Briefly, 3.9 g of 1-bromodococane and 17.2 g N,N,N',N'-tetramethyl-1,6-diaminohexane were dissolved in a 100 mL toluene/acetonitrile (50/50) solution with vigorous stirring at 60°C for 12 h. The mixture was then cooled, crystallized, filtered and washed with diethyl ether. Subsequently, 5.6 g of the resulting product and 1.5 g of 1-bromohexane was dissolved in 40 mL of acetonitrile. The mixture was then heated at 60°C for 12 h. After filtering and washing, the solid fraction was dried in a vacuum oven at 50°C to a constant weight, yielding a white solid designated as $\text{C}_{22-6-6}\text{Br}_2$.

MFI zeolite was hydrothermally synthesized using $C_{22-6-6}Br_2$ as the SDA. Initially, 2.2 g of $C_{22-6-6}Br_2$ was dissolved in 18.0 mL NaOH aqueous solution (1.0 mol L^{-1}). 0.02 g $Al_2(SO_4)_3 \cdot 18H_2O$ was dissolved in 18.0 mL H_2SO_4 acid solution (0.3 mol L^{-1}), then, it was added dropwise to the above alkaline solution under vigorous stirring. TEOS was subsequently introduced into the clarified solution and stirred vigorously at 90°C for 8 h to form a white gel with a molar composition of 60 NaOH: 1 $Al_2(SO_4)_3 \cdot 18H_2O$: 100 TEOS: 10 $C_{22-6-6}Br_2$: 18 H_2SO_4 : 4000 H_2O . The gel was transferred to a 250 mL stainless steel autoclave and crystallized for 120 h in an oil bath at 150°C . After crystallization, the zeolite precursors were washed with deionized water and dried at 120°C overnight. The sample was then calcined at 550°C for 8 h to remove the organic material, after that, it was ion-exchanged three times at 40°C for 6 h with a 1.2 mol L^{-1} NH_4NO_3 solution and then calcined at 550°C for 4 h to generate the H^+ form of the zeolite. The final product was designated as MFI-ns. Ni_{20} /MFI-ns catalysts, with a Ni mass content of 20 wt.%, was prepared by the impregnation-reduction method. Specifically, 1.7 g $Ni(NO_3)_2 \cdot 6H_2O$ was dissolved in 1.6 g deionized water. The mixture was added to 1.0 g of the MFI-ns support, impregnated for 12 h, dried at 120°C , and then calcined at 550°C for 4 h in air. Subsequently, the sample was reduced at 550°C for 4 h at a heating rate of $10 \text{ }^\circ\text{C min}^{-1}$ in H_2 , yielding the Ni_{20} /MFI-ns catalyst.

For comparison, Ni_{20} /SBA-15 and Ni_{20} /ZSM-5 catalysts were prepared using a method similar to that used for Ni_{20} /MFI-ns.

Characterizations

A Bruker D8 Advance Multiflex X-ray Powder Diffractometer (XRD) from

Germany was used to analyze the crystal phase structure of the catalyst samples.

The specific surface area, pore size distribution and pore volume of the catalysts were characterized using a Micrometric ASAP 2460 automatic gas adsorption apparatus. The total specific surface area was determined by the Brunauer-Emmett-Teller (BET) method. Mesopore pore volume and pore size distribution were calculated employing the Barrett-Joyner-Halenda (BJH) method based on the adsorption branch data, while the pore size distribution was further analyzed using the Nonlocal density functional theory (NLDFT) model.

The surface morphology of the catalysts was examined with a Hitachi SU 8220 field emission scanning electron microscope (SEM). Transmission electron microscopy (TEM) images were acquired using a Rigaku JEOL JEM-2100 F electron microscope operated at 200 kV.

Ultraviolet-visible photometer (UV-Vis) was recorded on a Hitachi U-3900H with a scan range of 500-200 nm.

Temperature-programmed reduction of H₂ (H₂-TPR) was conducted using a TP-5080 apparatus equipped with a thermal conductivity detector (TCD). Initially, 0.1 g of catalysts was pretreated in an Ar flow (50 mL min⁻¹), with the temperature ramped from 50-200°C at a rate of 10 °C min⁻¹ and maintained for 1 h. Subsequently, catalyst reduction was performed in a 10% H₂/Ar flow (50 mL min⁻¹) for 2 h, after which the flow rate was adjusted to 30 mL min⁻¹. The temperature was ramped to 900°C at a rate of 10 °C min⁻¹ while continuously recording the signal using TCD.

The acidic sites on the catalyst surface were determined by the temperature-

programmed desorption of NH_3 (NH_3 -TPD) using a Micromeritics AutoChem II 2920 spectrometer. 0.1 g of sample was pretreated in He (30 mL min^{-1}) with the temperature increasing from 50 to 200°C at $10^\circ\text{C min}^{-1}$, maintained for 0.5 h, and then cooled to 50°C . NH_3 adsorption was performed in a 5% NH_3 + 95% He flow until the baseline stabilized. Desorption of NH_3 was then carried out in a He flow (30 mL min^{-1}), with the temperature increasing to 100°C at $10^\circ\text{C min}^{-1}$ for 0.5 h, and then sequentially to 800°C at $10^\circ\text{C min}^{-1}$ while continuously recording the signal with TCD.

X-ray photoelectron spectroscopy (XPS) was performed using a Thermo Fischer, ESCALAB 250 Xi, USA to determine the electronic state of the metal in the catalyst.

Lignin Separation

The organosolv lignins were separated from the biomass according to the procedures shown in previous work ⁴. Briefly, bagasse (10.0 g) was combined with ethanol (120 mL) and 25 mL H_2SO_4 solution (0.3 mol L^{-1}) in a 250 mL stainless steel autoclave. The reactor was heated at 110°C for 4 h. After cooling, the mixture was filtered, and the filtrate was precipitated by adding water (200 mL). The resulting precipitated solid was separated by using a $0.22 \mu\text{m}$ membrane, and then dried under vacuum at 60°C until constant weight. The organosolv bagasse lignin was then obtained. Other lignins were achieved by a same procedure except for the raw lignocellulosic biomass.

Catalytic Hydrogenolysis of Lignin

The catalytic hydrogenolysis of lignin was carried out in a 50 mL stainless steel autoclave with a mechanical stirring device (Shanghai LABE Instrument Co., Ltd). Typically, 0.1 g of bagasse lignin and 50 mg of catalyst were added into 20 mL of

ethanol. The reactor was purged three times with H₂ for air displacement and pressurized to 2.0 MPa with H₂. Subsequently, the mixture of lignin, catalyst and solvent were heated to 270°C for 4 h.

After reaction, the mixture was separated into solid and liquid fractions by filtration. The solid fraction was washed with ethanol and dried at 110°C to a constant weight. Subsequently, it was calcined at 550°C for 4 h, and reduced in a flowing H₂ at 550°C for another 4 h. The obtained solid, which was designated as the recovered catalyst, was directly used in the next run of lignin hydrogenolysis. The liquid products were qualitatively and quantitatively analyzed on an Agilent 7890B/5977A gas chromatograph equipped with a mass spectrometry and flame ionization detector (GC-MS-FID). A 30 m × 0.25 mm × 0.25 μm HP-INNOWAX column was employed for product separation. Dimethyl phthalate was utilized as the internal standard, with corrections applied for the effective carbon number and the various functional groups present (*e. g.*, hydroxyl, ester, methoxy) ^{5,6}. Additionally, 250 mL of deionized water was added to the liquid fraction for precipitating the partly-decomposed or undecomposed lignin, which was then dried in a vacuum overnight until a constant weight was achieved. The resulting lignin was designated as Re-lignin. The lignin conversion, product yield, and selectivity were calculated according to the Eqs. (1)-(3):

$$\text{Conversion (\%)} = \left(1 - \frac{M_R}{M_0}\right) \times 100\% \quad (1)$$

$$\text{Yield (wt.\%)} = \frac{M_P}{M_0} \times 100\% \quad (2)$$

$$\text{Selectivity (\%)} = \frac{M_D}{M_P} \times 100\% \quad (3)$$

Where M_0 , M_R , M_P , and M_D are the weights of original lignin, Re-lignin, volatile products, and ethyl 4-hydroxyhydrocinnamate, respectively.

Calculation of theoretical maximum H-E yield

The maximum yield of **H-E** ($Y_{\text{H-E}}$) were calculated according to the Eq. (4):

$$Y_{\text{H-E}} (\text{wt.}\%) = \frac{M_0 \times C_{p\text{CA}0} - M_R \times C_{p\text{CAR}}}{M_0} \times \frac{M_{\text{H-E}}}{M_{p\text{CA}}} \times 100\% \quad (4)$$

$C_{p\text{CA}0}$ and $C_{p\text{CAR}}$ represent the contents of the *pCA* structural unit in original lignin and Re-lignin, respectively, which were acquired from the 2D HSQC NMR spectra (Table S9). $M_{p\text{CA}}$ represented the molecular mass of *pCA* unit, 164.16 g mol⁻¹, and $M_{\text{H-E}}$ represented the molecular mass of **H-E**, 194.23 g mol⁻¹.

Comparative Characterization of Lignin and Re-lignin

Fourier-transform infrared (FT-IR) spectroscopy of the lignin and Re-lignin were conducted using a Bruker Equinox-55 spectrophotometer, Germany, to determine the structural functional groups of lignin.

Elemental compositions (C, H, N and S) of lignin were conducted on an Elemental Various EL cube elemental analyzer, Germany. The content of oxygen (O) element was calculated by the principle of mass conservation based on the assumption that the samples only consist of C, H, N, S and O.

Gel permeation chromatography (GPC) analyses were performed to determine the molecular weight distribution of the lignin samples using an Agilent 1260 HPLC, USA. The analysis was conducted at 35°C using tetrahydrofuran as the eluent (1 mL min⁻¹), with an injection volume of 50 μL and a sample concentration of 1 mg mL⁻¹.

Two-dimensional heteronuclear single quantum coherence nuclear magnetic

resonance (2D-HSQC NMR) spectra of the lignin and Re-lignin samples were obtained using a Bruker Avance III 500 MHz NMR instrument. The central DMSO solvent peak was used as an internal reference (δ_C 39.5, δ_H 2.49 ppm)^{7,8}. The parameters were set as follows: ¹H spectral width was 5000 Hz; ¹³C spectral width was 20,000 Hz; hydrogen spectrum sampling was set to 2048 times with a relaxation time of 0.1 s; carbon spectrum sampling was 256 times with 72 scans.

Figures and Tables

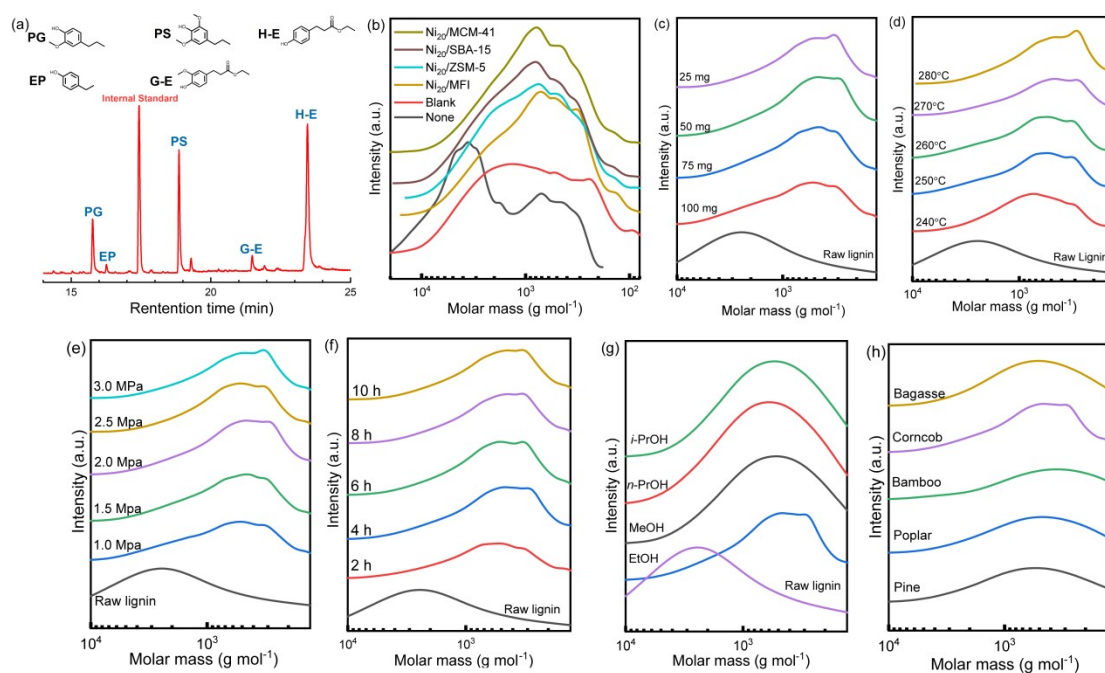


Figure S1. (a) GC-FID profile of lignin hydrogenolysis over Ni₂₀/MFI-ns under optimized conditions. The GPC spectra of (b) different catalysts samples, (c) catalyst dosage, (d) reaction temperature, (e) H₂ pressure, (f) reaction time, (g) different solvents, (h) different lignin samples of pine, poplar, bamboo, corncob, bagasse lignin.

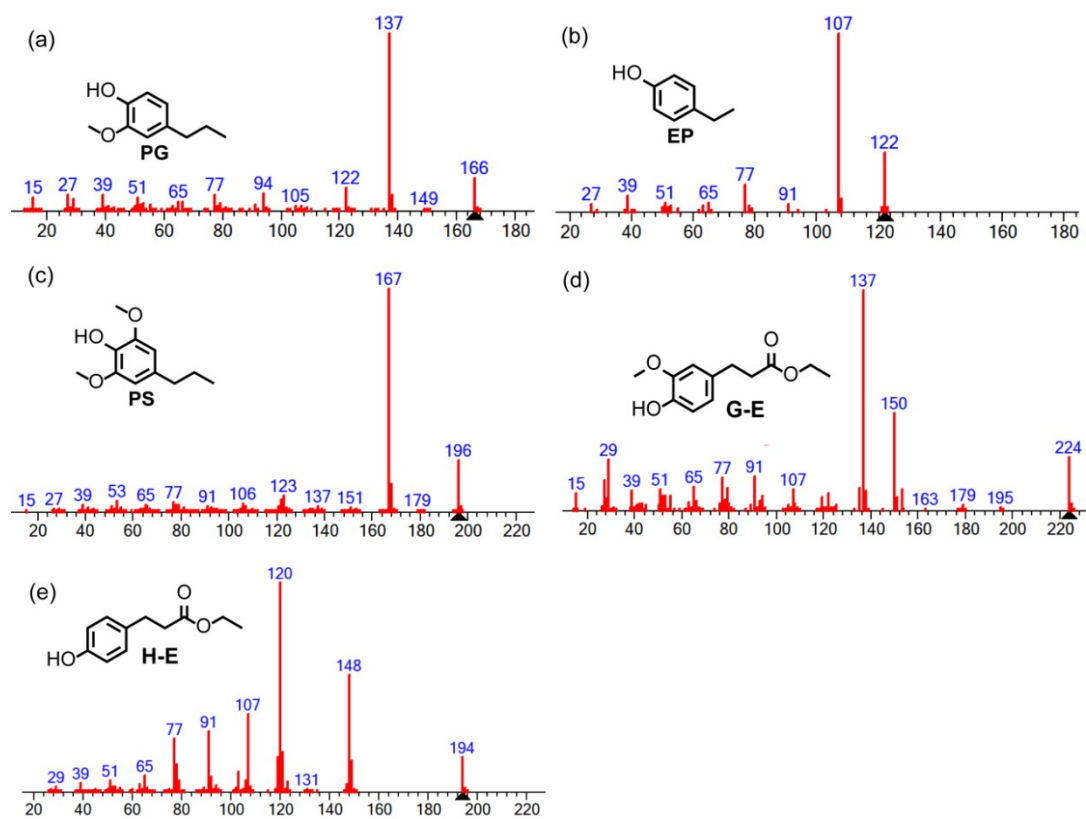


Figure S2. MS spectra of (a) **PG** ($m/z = 166$), (b) **EP** ($m/z = 122$), (c) **PS** ($m/z = 196$), (d) **G-E** ($m/z = 224$), and (e) **H-E** ($m/z = 194$) in lignin hydrogenolysis over Ni₂₀/MFI-ns under optimized conditions.

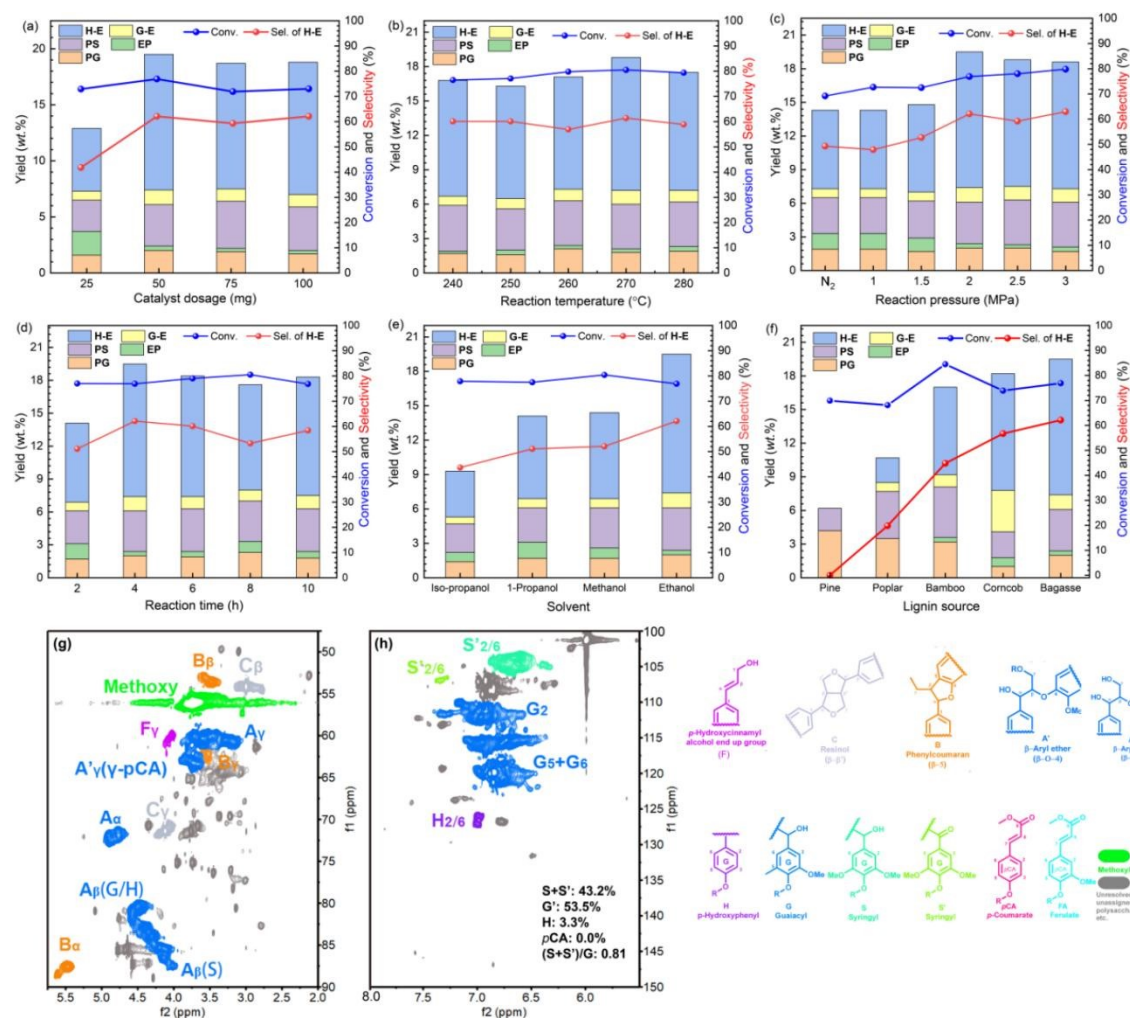


Figure S3. The effects of reaction conditions on lignin hydrolysis performance: (a) catalyst dosage, conditions: bagasse lignin (0.1 g), EtOH (20 mL), H₂ (3 MPa), 260°C, 4 h; (b) reaction temperature, conditions: bagasse lignin (0.1 g), Ni₂₀/MFI-ns (50 mg), EtOH (20 mL), H₂ (3 MPa), 4 h; (c) reaction time, conditions: bagasse lignin (0.1 g), Ni₂₀/MFI-ns (50 mg), EtOH (20 mL), H₂ (2 MPa), 270°C; (d) H₂ pressure, conditions: bagasse lignin (0.1 g), Ni₂₀/MFI-ns (50 mg), EtOH (20 mL), 270°C, 4 h; (e) solvent, conditions: bagasse lignin (0.1 g), Ni₂₀/MFI-ns (50 mg), EtOH (20 mL), H₂ (2 MPa), 270°C, 4 h; and (f) lignin resource, conditions: Ni₂₀/MFI-ns (50 mg), EtOH (20 mL), H₂ (2 MPa), 270°C, 4 h. 2D HSQC NMR spectra of organosolv pine lignin: (g) aliphatic region and (h) aromatic region.

As described in Fig. S3a, lignin conversion achieved the maximum value of 79.8%,

with a yield of **H-E** at about 9.8% when the catalyst dosage was 50 mg. Increasing the catalyst dosage slightly decreased the **H-E** yield, which is associated with the occurrence of condensation and over-hydrogenation ⁹. Increasing the reaction temperature from 240°C to 270°C raised lignin conversion to 80.5%, and the yield and selectivity of **H-E** reached the highest values of 11.6% and 61.4%, respectively (Fig. S3b). Excessively high reaction temperature caused lower yields of volatile products and **H-E**, which is related to the intermediates condensing to form coke and interunit C-C linkages with higher bond energy ¹⁰, as well as decarboxylation, hydrogenolysis and repolymerization of **H-E** ¹¹. Notably, the reaction proceeded even under 2.0 MPa N₂, yielding 7.4 wt.% of **H-E** and 14.6 wt.% of total monomers, similar to results obtained under 1.0 MPa H₂ (Fig. S3c). This suggests the hydrogen reforming from ethanol can facilitate lignin hydrogenolysis in the presence of Ni₂₀/MFI-ns. The highest yield of **H-E** (12.1 wt.%) and total yield of volatile products (19.5 wt.%) were obtained at 2.0 MPa H₂. Under such a H₂ pressure, Re-lignin with a low molecular weight (917 g mol⁻¹) was also generated (Fig. S1e). Increasing the H₂ pressure to 3.0 MPa caused the **H-E** yield and total yield to decrease (11.3 and 18.9 wt.%, respectively). A similar parabolic trend was also observed at variable reaction times (Fig. S3d). Shorter reaction time resulted in lower yield of **H-E** and total monomers (2 h, 7.2 wt.% and 14.1 wt.%, respectively) and higher *M_w* values (1188 g mol⁻¹) in comparison to a 4 h reaction time (4 h, 12.1 wt.%, 19.5 wt.% and 917 g mol⁻¹). Prolonging the reaction time to 10 h decreased the yields of **H-E** (10.8 wt.%) and monomers (18.3 wt.%).

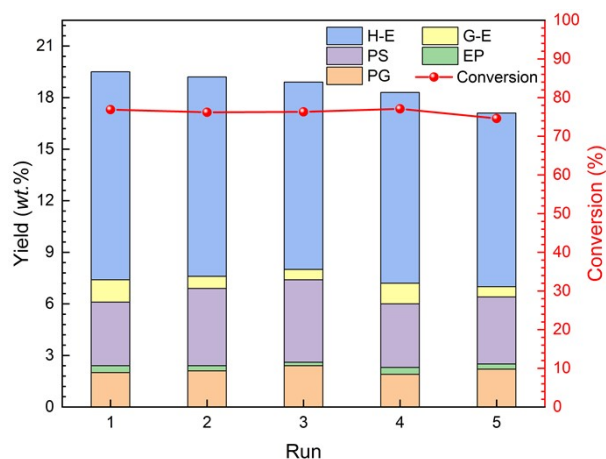


Figure S4. The recyclability of Ni₂₀/MFI-ns on lignin depolymerization. Reaction conditions: bagasse lignin (0.1 g), Ni₂₀/MFI-ns (50 mg), EtOH (20 mL), H₂ (2 MPa), 270°C, 4 h.

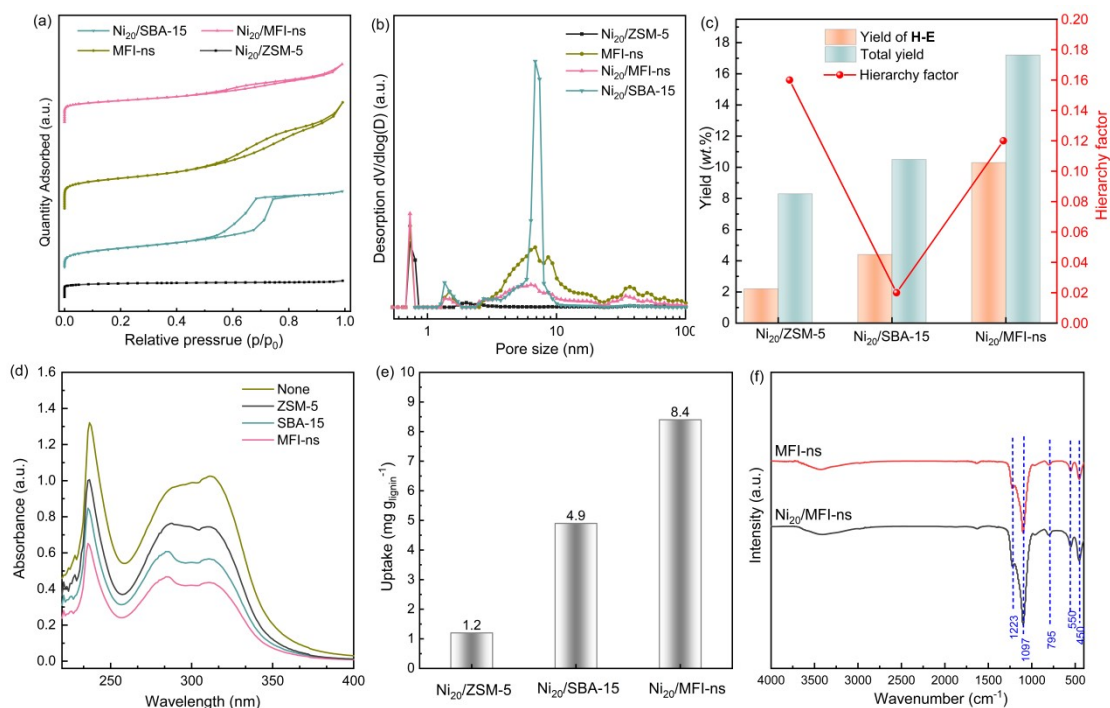


Figure S5. (a) N₂ adsorption/desorption isotherms. (b) pore size distribution. (c) Correlation between catalyst activity and Hierarchy factor. (d) UV-vis spectra for the filtrate of the mixed lignin and support suspension in THF. (e) Static adsorption content of lignin over different supports. Experiment: 0.1 g of support was added to 20 mL of solution (0.18 g L⁻¹) with stirring at ambient temperature. The centrifuged filtrate was analyzed by UV-vis spectroscopy. (f) FT-IR spectra of MFI-ns and Ni₂₀/MFI-ns.

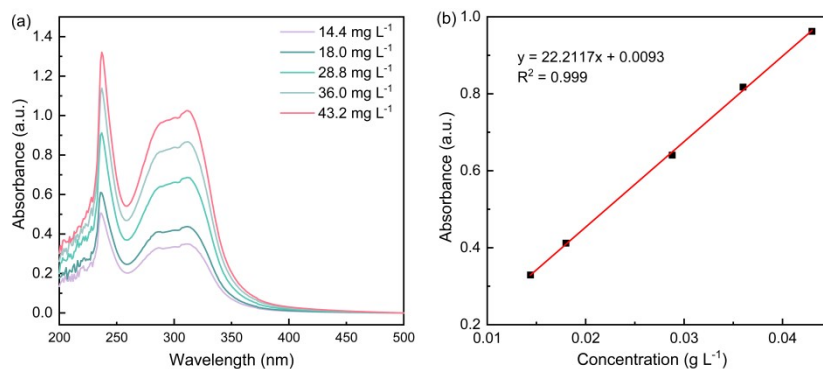


Figure S6. (a) UV-vis spectra for the lignin in THF. (b) Standard curves at 280 nm.

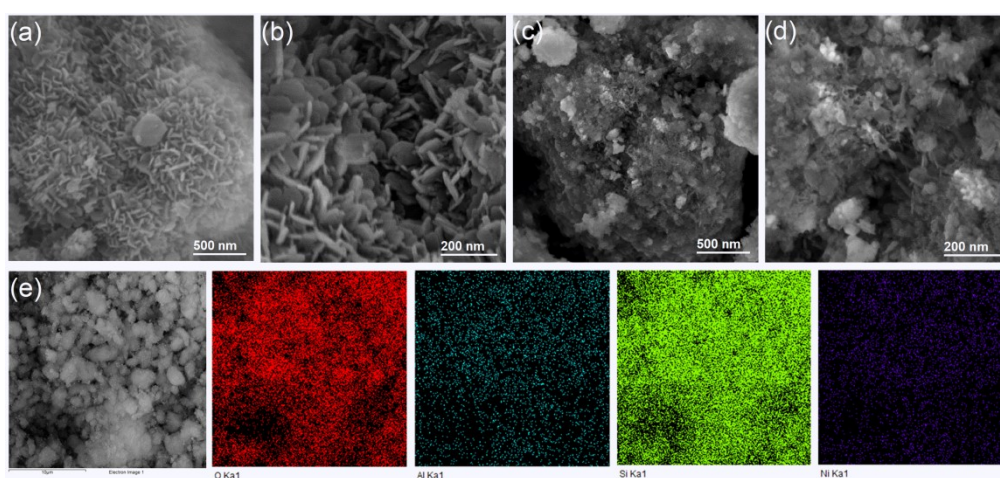


Figure S7. SEM images of (a, b) MFI, (c, d) Ni₂₀/MFI and (e) SEM EDS Mapping of Ni₂₀/MFI-ns.

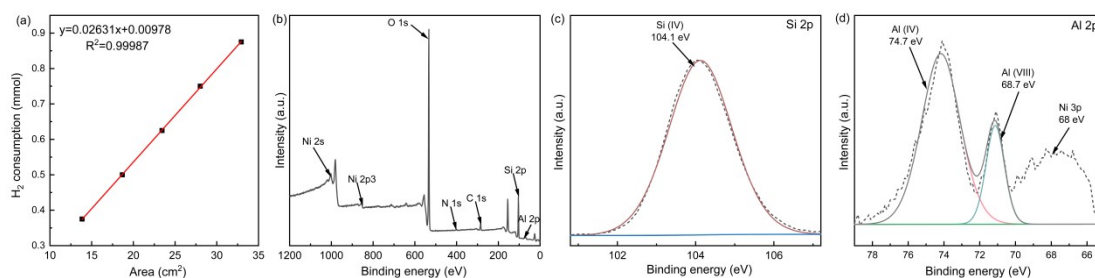


Figure S8. (a) Standard curves of H₂ consumption. (b) XPS survey, (c) Si 2p, and (d) Al 2p of Ni₂₀/MFI-ns.

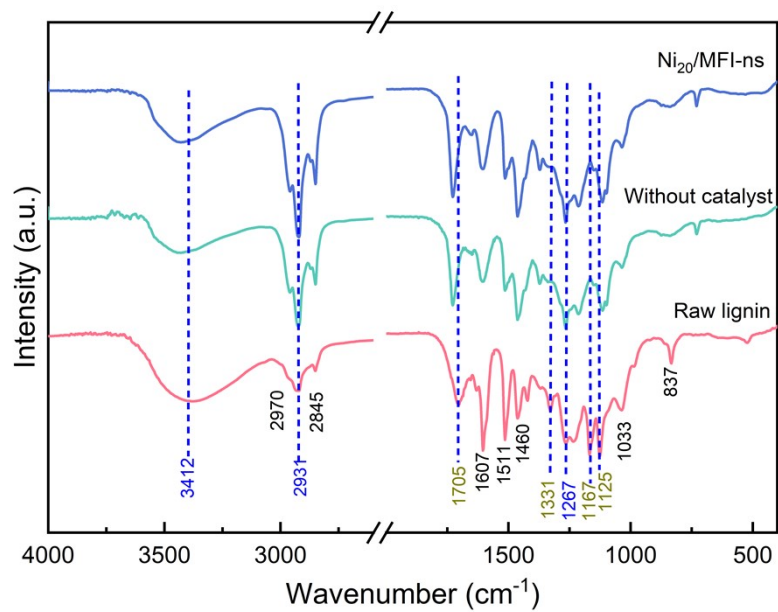


Figure S9. FT-IR spectra of raw lignin and recovered lignin over Ni₂₀/MFI-ns. Reaction conditions:

bagasse lignin (0.1 g), catalyst (50 mg), EtOH (20 mL), H₂ (2 MPa), 270°C, 4 h.

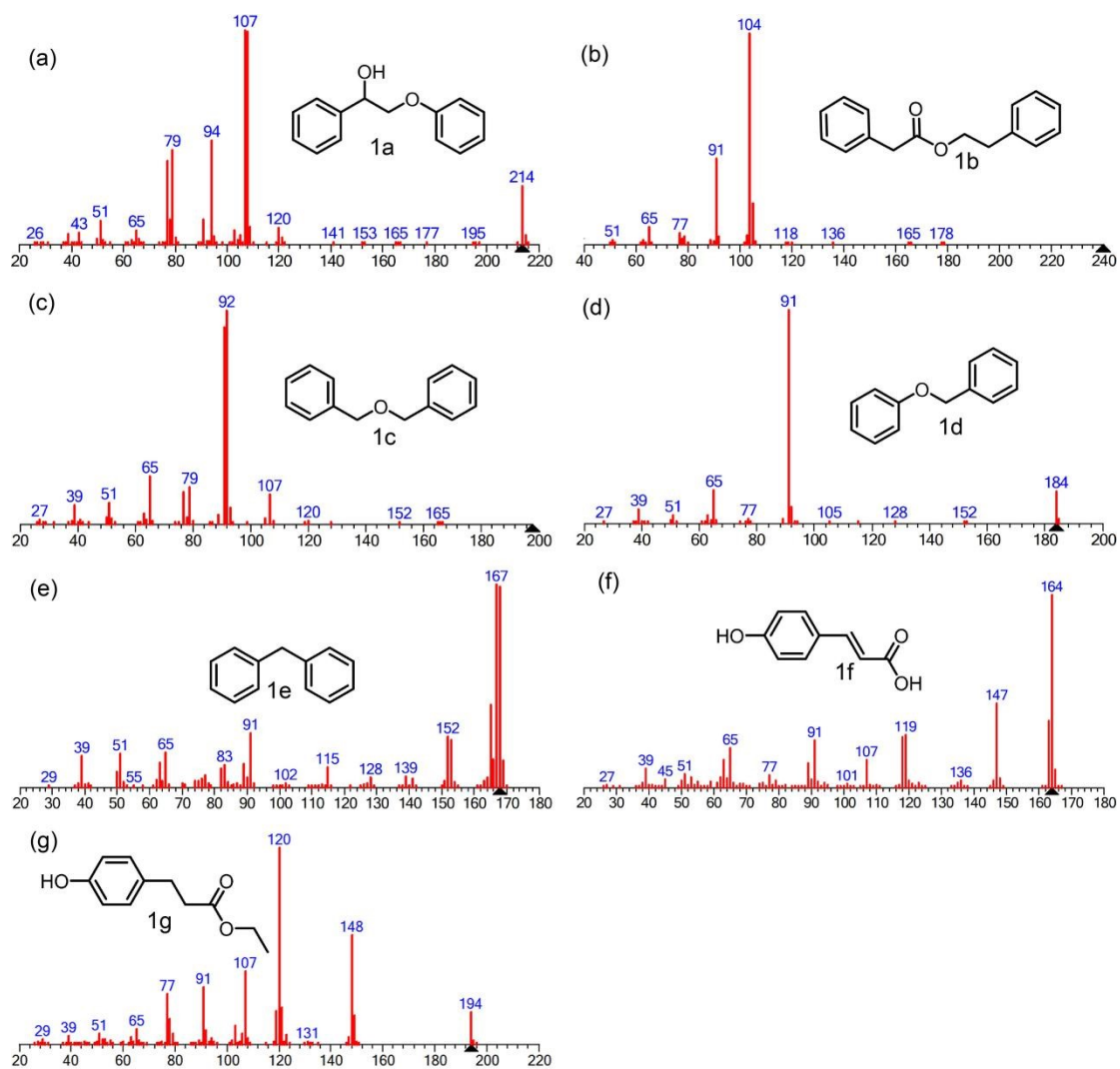
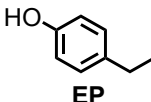
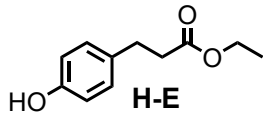
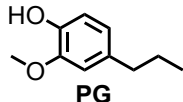
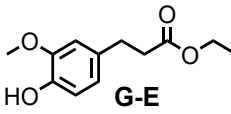
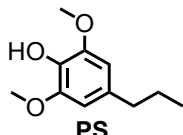


Figure S10. MS spectra of (a) **1a** ($m/z = 214$), (b) **1b** ($m/z = 240$), (c) **1c** ($m/z = 200$), (d) **1d** ($m/z = 184$), and (e) **1e** ($m/z = 167$), (f) **1f** ($m/z = 164$), (g) **1g** (**H-E**, $m/z = 194$) in lignin hydrogenolysis over $\text{Ni}_{20}/\text{MFI}$ -ns under optimized condition.

Table S1. The components of the monophenol products under optimized condition ^a

Retention time (min)	Components	Yield (wt.%)
	H units	12.5
16.28	 EP	0.4
23.36	 H-E	12.1
	G units	3.3
15.81	 PG	2.0
21.43	 G-E	1.3
	S units	3.7
18.93	 PS	3.7
	Total	19.5

^a Reaction conditions: 0.1 g bagasse lignin, 50 mg Ni₂₀/MFI, 270°C, 4 h, 2 MPa H₂.

Table S2. Textural analysis of different catalysts

Sample	Specific surface area (m ² g ⁻¹)			Pore volume (cm ³ g ⁻¹)			<i>HF</i> ^a
	S _{BET}	S _{Micro}	S _{External}	V _{Total}	V _{Meso}	V _{Micro}	
MFI-ns	479	168	311	0.64	0.55	0.09	0.09
Ni ₂₀ /MFI-ns	346	139	207	0.36	0.29	0.07	0.12
Ni ₂₀ /ZSM-5	216	164	52	0.12	0.04	0.08	0.16
Ni ₂₀ /SBA-15	327	25	308	0.53	0.52	0.01	0.02

^a Hierarchy factor (*HF*) is described as the product of $(V_{\text{micro}}/V_{\text{total}}) \times (S_{\text{ext}}/S_{\text{total}})$.

Table S3. The reduction temperature, relative area and H₂ consumption of the Ni_x/MFI-ns catalysts.

Catalyst	The reduction temperature (°C) and peak area			H ₂ consumption (mmol)	
	390°C	450°C	above 500°C	Experimental	Theoretical
Ni ₁₀ /MFI-ns	381.89	453.09	569.69	0.11	0.13
	1.00	3.27	0.45		
Ni ₁₅ /MFI-ns	371.56	423.12	512.22	0.17	0.15
	1.61	3.41	0.50		
Ni ₂₀ /MFI-ns	376.12	423.37	513.96	0.22	0.20
	3.47	3.14	0.78		
Ni ₂₅ /MFI-ns	364.62	411.05	532.37	0.28	0.23
	4.10	3.88	0.66		

Table S4. The desorption temperature, relative area and the ratio of acid sites of the catalysts.

Catalysts	The desorption temperature (°C) and peak area					Peak area and the ratio of acid sites (%)		
	A	B	C	D	E	Weak acid	Moderate acid	Strong acid
	MFI-ns	191.0 0.7	218.4 1.7	262.9 2.2	336.8 3.1	509.8 3.3	2.4 (22.2)	5.1 (47.2)
Ni ₁₀ /MFI-ns	115.7 0.6	144.9 1.1	205.4 3.0	363.6 2.5	557.5 2.6	1.7 (17.3)	5.5 (56.1)	2.6 (26.5)
Ni ₂₀ /MFI-ns	123.6 0.5	153.0 1.3	206.0 2.1	282.7 1.7	364.1 1.8	1.8 (24.3)	5.6 (75.7)	/ (0.0)
Ni ₂₅ /MFI-ns	107.4 0.6	135.3 1.2	175.7 2.0	241.5 2.7	409.6 3.3	3.8 (38.7)	6.0 (61.3)	/ (0.0)

Table S5. The Binding Energy (eV) and relative areas (%) of components (%) of Ni 2p.

Samples	Binding Energy (eV)					
	Ni 2p _{3/2}			Ni 2p _{1/2}		
	Ni ⁰	NiO	Ni(OH) ₂	Ni ⁰	NiO	Ni(OH) ₂
Ni ₁₅ /MFI- ns	853.4 (23.5)	857.7 (41.3)	862.3 (35.1)	870.5	873.3	876.1
Ni ₂₀ /MFI- ns	853.2 (35.7)	855.0 (35.0)	862.3 (29.4)	870.5	873.1	875.4
Ni ₂₅ /MFI- ns	853.1 (28.7)	854.3 (39.6)	861.5 (31.7)	870.2	872.2	874.8

Table S6. Average molecular weight of raw and recovered lignin^[a].

Sample	M_n (g mol ⁻¹)	M_w (g mol ⁻¹)	D
Raw lignin	1324	3729	2.8
Recovered lignin ^[b]	427	1556	3.6
Recovered lignin ^[c]	406	917	2.4

^[a] Reaction conditions: lignin 100 mg, catalyst 50 mg, EtOH 20 mL, 270°C, 4 h, 2 MPa H₂. ^[b]

Recovered lignin from reaction without catalyst, ^[c] Recovered lignin from reaction with Ni₁₂₀/MFI-ns.

Table S7. Elemental analysis of raw lignin, recovered lignin after reaction^[a]

Samples	Elemental content (wt.%)					Experimental	HHV ^[c]
	C	H	O ^[b]	N	S	molecular formula	(MJ Kg ⁻¹)
Raw lignin	61.39	5.94	32.04	0.44	0.19	C ₉ H _{10.45} O _{3.52} N _{0.06} S _{0.01}	24.02
Recovered lignin	70.66	8.24	20.74	0.36	0.00	C ₉ H _{12.59} O _{2.37} N _{0.05} S ₀	32.22

^[a] Conditions: 0.1 g of lignin, 50 mg of catalyst, 20 mL of EtOH, 2 MPa H₂, 270°C, 4 h. ^[b] Oxygen content is calculated by mass conservation based upon the assumption that the sample only contains C, H, S, N and O elements. ^[c] Evaluated by Dulong Formula: HHV (MJ kg⁻¹) = $0.335 \times [C] + 1.423 \times [H] - 0.154 \times [O] - 0.145 \times [N]$.

Table S8. Assignment of main lignin ^{13}C - ^1H cross-signals in the 2D HSQC NMR spectra ¹²⁻¹⁴

Lable	$\delta_{\text{C}}/\delta_{\text{H}}$ (ppm) ^[a]	Assignments
Methoxyl	56.11/3.72	C-H in methoxyls
A _{α}	72.25/4.89	C _{α} -H _{α} in β -O-4 units (A)
A _{β} (H/G)	80.33/4.49	C _{β} -H _{β} in β -O-4 substructures linked to H/G units (A)
A _{β} (S)	85.17/4.17	C _{β} -H _{β} in β -O-4 substructures linked to S units (A)
A _{γ}	60.31/3.50	C _{γ} -H _{γ} in β -O-4 substructures (A)
A(γ - <i>p</i> CA) _{γ}	63.80/4.36	C _{γ} -H _{γ} in γ - <i>p</i> CA of β -O-4 (A)
B _{β}	53.85/3.64	C _{β} -H _{β} in phenylcoumaran substructures (B)
B _{γ}	62.89/3.63	C _{γ} -H _{γ} in phenylcoumaran substructures (B)
C _{α}	83.57/5.00	C _{α} -H _{α} in resinol substructures (C)
C _{β}	53.40/3.47	C _{β} -H _{β} in resinol substructures (C)
C _{γ}	70.66/4.03	C _{γ} -H _{γ} in resinol substructures (C)
H _{2,6}	128.35/7.18	C _{2,6} -H _{2,6} in H units (H)
G ₂	111.73/6.94	C ₂ -H ₂ in guaiacyl units (G)
G ₆	120.00/6.78	C ₆ -H ₆ in guaiacyl units (G)
S _{2,6}	104.20/6.71	C _{2,6} -H _{2,6} in syringyl units (S)
S' _{2,6}	106.97/7.36	C _{2,6} -H _{2,6} in oxidized S units (S')
<i>p</i> CA _{2,6}	130.68/7.48	C _{2,6} -H _{2,6} in <i>p</i> -coumarate (<i>p</i> CA)
<i>p</i> CA _{3,5}	115.91/6.94	C _{3,5} -H _{3,5} in <i>p</i> -coumarate (<i>p</i> CA)
<i>p</i> CA ₇	144.92/7.30	C ₇ -H ₇ in <i>p</i> -coumarate (<i>p</i> CA)
<i>p</i> CA ₈	113.52/6.27	C ₈ -H ₈ in <i>p</i> -coumarate (<i>p</i> CA)
FA ₂	111.60/7.35	C ₂ -H ₂ in ferulate (FA)
FA ₆	123.26/7.15	C ₆ -H ₆ in ferulate (FA)
FA ₇	144.97/7.31	C ₇ -H ₇ in ferulate (FA)

^[a] $\delta_{\text{C}}/\delta_{\text{H}}$ (ppm) are the chemical shifts of C-H bond in lignin, which is summarized from the existing literatures.

Table S9. Integrated results of monomers and linkages in bagasse lignin based on the 2D HSQC

NMR.

Linkage	$P_{(\beta-O-4)}/\%$	$P_{(\beta-5)}/\%$	$P_{(\beta-\beta)}/\%$	$P_{(pCA)}/\%$	$P_{(EE)}/\%$	(S+S')/(G+FA)/(H+pCA)
Raw lignin	64.9	24.6	0.3	23.6	--	34.1/38.2/27.7
Re-lignin	0	0	1.3	12.3	2.0	30.0/43.0/28.1

$$(S+S') : (G+FA) : (H+pCA) = (0.5I_{(S_{2,6})} + 0.5I_{(S'_{2,6})}) : (I_{(G_2)} + I_{(FA_2)}) : (0.5I_{(H_{2,6})} + 0.5I_{(pCA_{2,6})});$$

$$I_{C_9 \text{ units}} = 0.5I_{(S_{2,6})} + 0.5I_{(S'_{2,6})} + I_{(G_2)} + I_{(FA_2)} + 0.5I_{(H_{2,6})} + 0.5I_{(pCA_{2,6})};$$

$$P_x(\%) = I_x / I_{C_9} \times 100$$

$$Y_{H-E} = 20.6 \text{ wt.}\%$$

Table S10. Summary of the FT-IR bands observed in lignin ^{15, 16}

Entry	Wavenumbers (cm ⁻¹)	The attributions of the main absorptions
1	3406	-OH stretching
2	2970	C-H symmetry stretching in methyl groups
3	2932	C-H asymmetry stretching in methylene groups
4	2845	-CH ₃ symmetry stretching in methoxy groups
5	1705	C=O stretching in unconjugated ketone, carbonyl and in ester groups
6	1634	C=C stretching
7	1604	aromatic skeletal vibrations plus C=O stretching
8	1512	aromatic skeletal vibrations
10	1420	aromatic skeletal vibrations
11	1328	C-O of S-ring
12	1267	G-ring plus C=O Stretching
13	1222	C-C, C-O and C=O stretching; G condensed >G etherified
14	1167	C=O in ester groups
15	1123	C-H in-plane deformation in S-ring
16	1031	Aromatic C-H in-plane deformation (G>S) plus C-O deformation in primary alcohols, C=O stretching
17	981	C=O in lignin-carbohydrate complexes (LCC)
18	916	aromatic C-H out-of-plane
19	833	C-H out-of-plane in position 2,5,6 of G unit

References

1. K. Na, M. Choi, W. Park, Y. Sakamoto, O. Terasaki and R. Ryoo, *J. Am. Chem. Soc.*, 2010, **132**, 4169-4177.
2. L. Li, J. Kong, H. Zhang, S. Liu, Q. Zeng, Y. Zhang, H. Ma, H. He, J. Long and X. Li, *Appl. Catal., B*, 2020, **279**, 119343.
3. M. Choi, K. Na and J. Kim, *Nature*, 2009, **461**, 246-249.
4. J. Long, X. Li and B. Guo, *Catal. Today*, 2013, **200**, 99-105.
5. M. Kállai and J. Balla, *Chromatographia*, 2002, **56**, 357-360.
6. J. T. Scanlon and D. E. Willis, *J. Chromatogr. Sci.*, 1985, **23**, 333-340.
7. F. Gao, J. D. Webb, H. Sorek, D. E. Wemmer and J. F. Hartwig, *ACS Catal.*, 2016, **6**, 7385-7392.
8. X. Wu, X. Fan, S. Xie, J. Lin, J. Cheng, Q. Zhang, L. Chen and Y. Wang, *Nat. Catal.*, 2018, **1**, 772-780.
9. T. Phongpreecha, K. F. Christy, S. K. Singh, P. Hao and D. B. Hodge, *Bioresour Technol.*, 2020, **316**, 123907.
10. Z. Luo, Z. Zhu and R. Xiao, *Biomass Convers. Biorefin.*, 2022, **14**, 16631-16637.
11. V. T. Tran, T. M. Le, P. V. Vu, H. M. Nguyen, Y. H. P. Duong and P. K. Le, *Sci. World J.*, 2022, **2022**, 7872307.
12. Y. Wu, Z. Huang, K. Lv, Y. Rao, Z. Chen, J. Zhang and J. Long, *J. Agric. Food Chem.*, 2022, **70**, 5624-5633.
13. J. Kong, L. Li, Q. Zeng, J. Long, H. He, Y. Wang, S. Liu and X. Li, *Ind. Eng. Chem. Res.*, 2021, **60**, 17897-17906.
14. H. Li, X. Zheng, H. Zhang, X. Li and J. Long, *ACS Sustain. Chem. Eng.*, 2020, **8**, 15685-15695.
15. S. Kubo and J. F. Kadla, *Biomacromolecules*, 2005, **6**, 2815-2821.
16. X. Lin, L. Chen, H. Li, Y. Lv, Y. Liu, X. Lu and M. Liu, *Bioresour. Technol.*, 2021, **333**, 125136.